Arabian Journal of Chemistry (2021) **14**, 103180

King Saud University

Arabian Journal of Chemistry

www.ksu.edu.sa
www.sciencedirect.com

ORIGINAL ARTICLE

Photocatalytic degradation of Rhodamine B (RhB) dye in waste water and enzymatic inhibition study using cauliflower shaped ZnO nanoparticles synthesized by a novel One-pot green synthesis method

Shashanka Rajendrachari [a,*], Parham Taslimi [b,*], Abdullah Cahit Karaoglanli [a], Orhan Uzun [c,d], Emre Alp [a], Gururaj Kudur Jayaprakash [e]

[a] *Department of Metallurgical and Materials Engineering, Bartin University, Bartin 74100, Turkey*
[b] *Department of Biotechnology, Faculty of Science, Bartin University, Bartin 74100, Turkey*
[c] *Rectorate of Bartin University, Bartin, Turkey*
[d] *Ankara University, Department of Physics, Ankara, Turkey*
[e] *Faculty of Basic Sciences, School of Chemistry, Shoolini University, Bajhol, Himachal Pradesh 173229, India*

Received 28 March 2021; accepted 18 April 2021
Available online 26 April 2021

KEYWORDS

ZnO nanoparticles;
Green synthesis;
Alchemilla vulgaris;
Metabolic enzyme inhibition;
Photocatalytic;
Rhodamine B

Abstract The ZnO nanoparticles (NPs) are considered to be one of the inexpensive and very important bioactive materials widely used in drug delivery, as a photo-catalyst material, antibacterial, bioimaging, anticancer, anti-inflammation, wound healing, and diabetes treatment. Therefore, we have prepared ZnO NPs using *Alchemilla vulgaris* (Lady's mantle) leaves and investigated their anti-enzymatic properties. Phases of the ZnO NPs were determined from X-Ray diffraction (XRD) spectra. The shape and size of the green synthesized NPs were investigated by scanning electron microscopy (SEM) and it confirms the cauliflower shape with an average size of 120 nm. But the beads inside the cauliflower shape are 20 nm in size. The prepared ZnO NPs show the cumulative median particle size of 550 nm. The thermogravimetric (TG) and differential thermal analysis (DTA) were performed at different heating rates to study the percentage of weight loss, and activation energy. The activation energy was calculated to be 4.98 kJ/moles using Kissinger method. We also studied the enzyme inhibition effect of ZnO NPs containing biologically active groups on

* Corresponding authors.
E-mail addresses: shashanka@bartin.edu.tr (S. Rajendrachari), ptaslimi@bartin.edu.tr, parham_taslimi_un@yahoo.com (P. Taslimi).

Peer review under responsibility of King Saud University.

ELSEVIER Production and hosting by Elsevier

https://doi.org/10.1016/j.arabjc.2021.103180

important metabolic enzymes like butyrylcholinesterase(BChE), acetylcholinesterase (AChE) and α-glycosidase (α-Gly) enzymes. The bandgap of ZnO NPs was also studied by UV–Vis spectroscopy via Tauc's method and it was determined to be 3.27 eV. The photocatalytic property of the ZnO NPs was executed against rhodamine B (RhB) under the illumination of an AM 1.5 solar simulator.

1. Introduction

The recent past had witnessed numerous foremost innovations in the field of nanotechnology with an acceleration speed (Mirzaeia and Darroudi, 2017). Researchers are developing a variety of nanoparticles with improved properties depending upon their types, methods, morphology, size, crystal structures, etc. (Reddy et al., 2012; Rajendrachari et al., 2013; Shashanka, 2017, 2019). The nanomaterials made up of metals, metal oxides (MO's), nano-graphenes, carbon nanotubes, and nano-composites are the most important nanomaterials can be prepared from different methods with utmost specificity. Among them, the research on MO nanoparticles are marching with significant speed because of their extremely small size, greater surface area, simple preparation methods, unique properties and applications (Hareesha et al., 2019). Generally, they are prepared from chemical, physical and biological methods. But, we have prepared them from biological methods due to its fast, robust, non-toxic nature, and do not require high-priced equipment and special chemicals unlike physical and chemical methods. The plant mediated green synthesise of MO nanoparticles is one of the popular biological method and advantageous due to the wide availability and biodiversity of flora. All the plants consists of phytochemicals such as phenols, flavonoids, aldehydes, and ketones; they converts metal salts into metal oxide nanoparticles due to their reducing power (Shashanka, 2020).

The present method is a one-pot synthesis which improves the reactivity of the reaction in just one pot or glassware or a reactor. This method also reduced the elongated extraction, separation, purification processes. Therefore, one-pot synthesis is becoming more popular and having plenty of advantages over other methods. Hence we have prepared ZnO NP's using one-pot synthesis green method.

Boroja et al. (2018) studied the amount of different phytochemicals present in *Alchemilla vulgaris* and reported the high content of phenolic compounds. This enhances their antioxidant capacity, metal chelation, reducing power, enzyme inhibition properties, etc. Therefore, one can expect that the metal oxide nanoparticles prepared from *Alchemilla vulgaris* (Lady's mantle) exhibits excellent enzyme inhibition properties. Hence we studied the enzyme inhibition properties of ZnO NP's in the present paper.

The bio-functional nanomaterials like ZnO have caught the attention of biomedical researchers due to their antibacterial, anti-inflammation, anticancer, drug delivery, diabetes treatment, bio-safe, biocompatibility, photo-catalytic, structure-dependent, electrical, thermal transport properties, wound healing, and bio-imaging properties (Jiang et al., 2018). All these properties are majorly depends on the particle size, morphology, methods of preparation, orientation and ratio (Knoll and Keilmann, 1999; Liz-Marzán et al., 1996). Plant mediated synthesis of ZnO NP's is preferred over other biological methods due to the combined biomedical properties of both plant extract and the nanoparticles. In the present paper biomedical properties of *Alchemilla vulgaris* (Lady's mantle) further improves the properties of ZnO NP's. Literatures on the green synthesis of ZnO NP's by various plant leaves are available. But, no literature is reported on the preparation of the same using *Alchemilla vulgaris* (Lady's mantle) leaves extract.

The *Alchemilla vulgaris* is grows in the mountain regions of Europe, North America, Asia and belongs to the Rosaceae family (Tobyn et al., 2011). The plant is specially cultivated for its medicinal properties like anticoagulant, anti-bleeding, anti-inflammatory, antimicrobial, antioxidant properties, and for its wonderful healing power (Tobyn et al., 2011). There are 541 *Alchemilla* species were registered in Europe and the Mediterranean; Turkey registered with 74 varieties of *Alchemilla* species majorly found at the northern and the eastern part of Anatolia.

The plant mediated synthesis of nanomaterials can significantly bring greater green revolution for nanomaterial industries where environmental contamination is an important concern (Gültekin et al., 2016). Many researchers are trying to improve this method by using different variety of flora and reaction conditions. Table 1 depicts the ZnO NP's prepared from different plants by various researchers followed by their important findings.

The prepared ZnO NPs are mainly used to inhibit the growth of various isoenzymes. One of the important biological effects of quinazolinone derivatives is to inhibit acetylcholinesterase (AChE) and butyrylcholinesterase (BChE) in brain which causes Alzheimer's disease (Biçer et al., 2019). Cholinesterase (ChE) enzymes mainly catalyzes the hydrolysis of the neurotransmitter ACh restoring the cholinergic pathway at the end of the nerve transmission in the centric neural system (Erdemir et al., 2019). The α-Glycosidase hydrolyzes the glycosidic bonds and converts di- or oligosaccharides into monosaccharides to help in the breakdown and absorption of sugars (Gulçin et al., 2018; Huseynova et al., 2019). Additionally, the green synthesized ZnO NP's are a strong potential candidate for inhibiting enzymes. Therefore, we studied the effect of ZnO NP's in inhibiting the some metabolic enzymes.

Additionally, the green synthesized ZnO NPs are also used as a photocatalyst to purify the wastewater from organic toxic pollutants like rhodamine-B. ZnO NPs, which has a direct wide bandgap and a large exciton binding energy (Özgür et al., 2015). Recently, ZnO nanomaterials used in photo-catalytic applications has emerged significantly in the field of environmental applications due to their impressive photo-catalytic activities (Kakarndee and Nanan 2018; Chankhanittha and Nanan 2018, 2021; Juabrum et al.,

Table 1 The ZnO nanoparticles prepared from different plants by various researchers.

Plant name	Precursor	Average size and morphology	Featured study	References
Deverra tortuosa	$Zn(NO_3)_2{\cdot}6H_2O$	9–31 nm and almost spherical shape	Cytotoxic Activity	(Selim et al., 2020)
Tecoma castanifolia	$ZnSO_4$	70–75 nm and spherical shape	Antioxidant, bactericidal and anticancer activities	(Sharmila et al., 2019)
Passiflora caerulea	$Zn(CH_3CO_2)_2{\cdot}2H_2O$	70 nm and spherical shape	Anti-bacterial activity against urinary tract infection	(Santhoshkumar et al., 2017)
Solanum torvum	$Zn(NO_3)_2{\cdot}6H_2O$	34–40 nm and spherical shape	Evaluation of the toxicological profile	(Ezealisiji et al., 2019)
Hibiscus subdariffa	$Zn(CH_3CO_2)_2{\cdot}2H_2O$	300–400 nm and Cauliflower shape	Anti-bacterial and anti-diabetic activity	(Bala et al., 2015)
Tectona Grandis	$Zn(NO_3)_2{\cdot}6H_2O$	54 nm and partially spherical	Anti-bacterial, anti-arthritic, anti-oxidant and in-vitro cytotoxicity activities	(Senthilkumar et al., 2017)
Sambucus ebulus	$Zn(CH_3CO_2)_2{\cdot}2H_2O$	25–30 nm and spherical	Antibacterial activity and a photocatalytic degradation of methylene blue dye pollutants	(Alamdari et al., 2020)
Peganum Harmala	$Zn(CH_3CO_2)_2{\cdot}2H_2O$	40 nm and spherical	Antibacterial activity	(Mehar et al., 2019)
Crocus sativus	$Zn(CH_3CO_2)_2{\cdot}2H_2O$	50 nm and spherical	The antibacterial effect was investigated against food pathogens	(Rahaiee et al., 2020)
Parthenium Hysterophorus	$Zn(NO_3)_2{\cdot}6H_2O$	16–45 nm and quasi-spherical, radial and cylindrical shape	Antibacterial studies	(Datta et al., 2017)
Pelargonium zonale	$Zn(NO_3)_2{\cdot}6H_2O$	50–60 nm and spherical	Antibacterial studies	(Vahidi et al., 2019)
Tilia Tomentosa	$Zn(NO_3)_2{\cdot}6H_2O$	80 nm and spherical	Dye-sensitized solar cell applications	(Shashanka et al., 2020)
Veronica multifidi	$Zn(CH_3CO_2)_2{\cdot}2H_2O$	10–100 nm and nearly hexagonal and quasi-spherical	Antimicrobial and antibiofilm activities	(Dogan and Kocabas, 2020)
Alchemilla vulgaris	$Zn(NO_3)_2{\cdot}6H_2O$	120 nm and cauliflower shape	Thermal, optical and enzymatic studies	(Present paper)

2019). Among the various techniques of Advanced Oxidation Processes (AOPs) to treat contaminated water, the heterogeneous photo-catalysis process is a promising, efficient, and environmental-friendly process to eliminate toxic pollutants, especially organic compounds which are degraded to harmless products or transform into less toxic (Ahmed and Haider 2018; Chankhanittha et al., 2021). The photocatalytic property of ZnO materials are utilized in the purification of wastewater from organic toxic pollutants via the heterogeneous photo-catalytic method (Chankhanittha et al., 2019, 2021; Senasu et al., 2021). Bhuyan et al. reported the photo-catalytic activity of biosynthesis of ZnO from *Azadirachta indica* against methylene blue (MB) under UV irradiation (Bhuyan et al., 2015) and Fu and Fu (2015) investigated biosynthesis of ZnO using leaf extract of *Plectranthus amboinicus* against methyl red (MR). In this study, by using *Alchemilla Vulgaris* leaves extract, we prepared ZnO NPs, which were then employed as a photo-catalyst for determining the degradation activity against rhodamine-B (RhB) organic molecule.

2. Experimental

2.1. Chemicals used

$Zn(NO_3)_2{\cdot}6H_2O$, NaOH and rhodamine B were purchased from Sigma-Aldrich. All the solutions and plant extract were prepared using RO water.

2.2. Plant extract of *Alchemilla vulgaris*

The leaves of *Alchemilla vulgaris* were purchased from the city market of Bartin, Turkey. Five grams of powdered *Alchemilla vulgaris* (Lady's mantle) leaves were weighed and boiled with 100 mL deionized water for 15 min till we get a dark yellow color. Then the solution was filtered to remove any suspended impurities and the aliquots of the solution can be stored at 5℃. This solution is called as plant extract and it serve as both reducing as well as capping agent. Using this plant extract we have prepared cauliflower shaped ZnO NP's. Fig. 1 shows the leaves of *Alchemilla vulgaris* (Lady's mantle), extract and colloidal solution of ZnO NP's.

2.3. Synthesise of cauliflower shaped ZnO NP's

Stir 2.972 g of Zinc nitrate hexahydrate in 100 mL distilled water for 5 min and later added 5 mL of extract till the solution turns yellow. Later, add 1 M NaOH drop by drop till pale yellow color precipitate appears. Centrifuge the solution for 10 min at 7500 rpm and wash the precipitate using water and centrifuge it at least 5 times. Collect the precipitates of ZnO NP's and dry them at 70℃ for 24 h followed by calcination at 400℃ for 15 min to vaporize the organic impurities. Allow calcined samples to cool down and hand pulverize them using mortar pestle (If needed). Fig. 2 depicts the experimental representation of ZnO NP's using *Alchemilla vulgaris* (Lady's mantle) leaves extract.

Fig. 1 **(a)** Leaves of *Alchemilla vulgaris* (Lady's mantle), **(b)** Plant extract and **(c)** Colloidal solution of ZnO NP's.

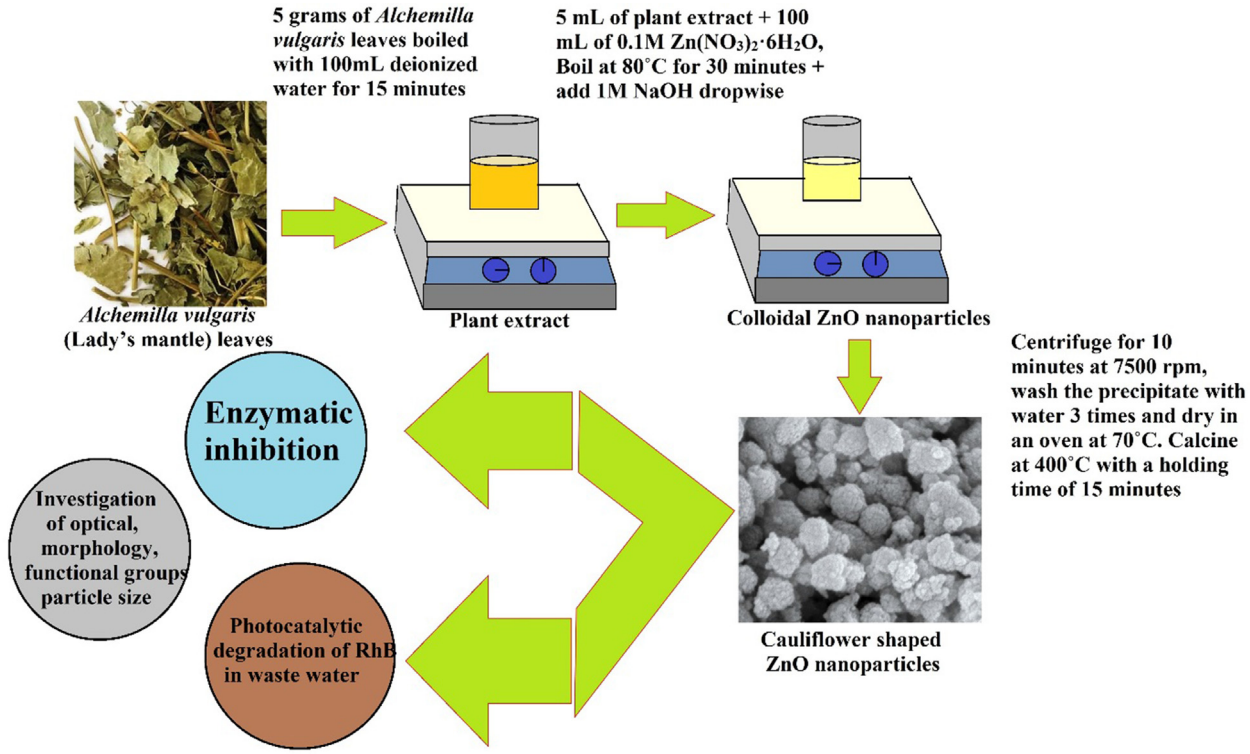

Fig. 2 The graphical representation of synthesis of cauliflower shaped ZnO NP's using *Alchemilla vulgaris* (Lady's mantle) leaves extract.

2.4. Bioactivity studies

BChI and AChI were used as reaction substrate molecules and DTNB was used to determine anticholinesterase activity by Ellman et al., (1961) method (Küçükoğlu et al., 2019; Kuzu et al., 2019). The inhibition effect of glycosidase of ZnO nanoparticle was studied using Tao et al., (2013) process. The 5 µL of the sample and the phosphate buffer (pH 7.4, 75 µL) was combined. After pre-incubation, 50 µL of p-Nitrophenyl-D glycopyranoside (p-NPG) was applied to the phosphate buffer (5 mM, pH 7.4) and re-incubated at 37 °C. The 3 different concentrations of ZnO NP's were used to de-terminate the Ki values (Taslimi and Gulçin, 2018; Taslimi et al., 2018).

2.5. Photocatalytic activity

Determining the photocatalytic performance of synthesized zinc oxide particles was executed against rhodamine B (RhB) organic dyes at ambient temperature in atmospheric conditions. The typical photo-catalytic testing dye solution used for determining the photocatalytic activity of synthesized particles was the concentration of 10 mg RhB per Litre. The 40 mg of ZnO NPs were dispersed in 80 mL of a prepared

aqueous RhB solution. Prior to illumination under a solar simulator, the dispersed solution was magnetically stirred in the dark for 1 h to confirm the adsorption/desorption equilibrium on the surface of the ZnO nanoparticles. Subsequently, the solution was then irradiated by using an AM1.5 filtered light with a 500 W xenon lamp SHBC XSS-5XD solar simulator under continuously magnetic stirring conditions. At a certain irradiation time interval, 3 mL samples were taken from the solution for the absorption spectra of the solution. After removing synthesized ZnO nanoparticles from an aqueous solution by centrifuge, the absorption characteristics of the solutions at a particular time were determined to measure the degradation rate of RhB organic dye by using a UV–Vis-NIR spectrophotometer.

3. Results and discussion

3.1. Phase analysis:

Fig. 3 depicts the XRD pattern of ZnO NP's prepared from *Alchemilla vulgaris* (Lady's mantle) leaves. The planes (100), (002) and (101) were present at 31.82°, 34.47°, and 36.28° diffraction peaks respectively as shown in the figure. This confirms the formation of hexagonal ZnO as confirmed by JCPDF Card No.: 01–070-8072. Even after calcination, the XRD peaks are broadened due to their refined size (Shashanka and Chaira, 2015a, 2015b), and high strain (Gupta et al., 2015; Shashanka et al., 2015; Nayak et al., 2016). The average crystallite size of ZnO NP's prepared from *Alchemilla vulgaris* (Lady's mantle) leaves was determined by Scherrer's formula (Shashanka and Chaira, 2014; Shashanka et al., 2015, 2016);

$$D = \frac{K\lambda}{\beta \cos\theta} \tag{1}$$

The crystallite sizes of ZnO NP's were calculated for (100), (002) and (101) planes respectively using equation (1) and it were found to be ~ 20 nm.

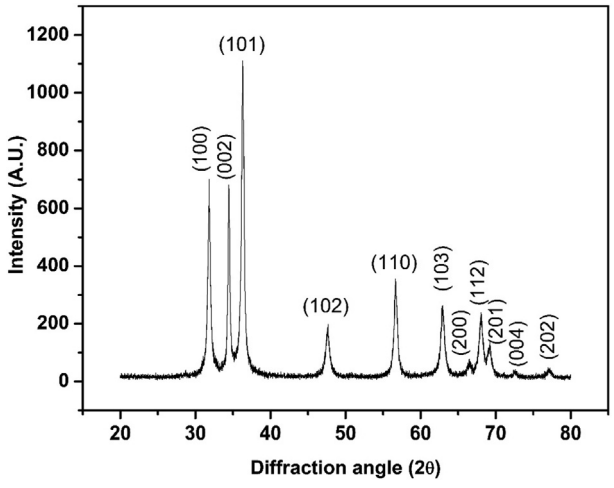

Fig. 3 X-ray diffraction (XRD) pattern of ZnO NP's synthesized from *Alchemilla vulgaris* (Lady's mantle) leaves.

3.2. Microstructure of ZnO NP's

The SEM microstructure of biosynthesized ZnO NP's prepared by *Alchemilla vulgaris* (Lady's mantle) leaves is shown in Fig. 4 (a). The SEM microstructure confirms the cauliflower shaped ZnO NP's with average size of 120 nm. But the beads inside the cauliflower shape exhibit the average particle size of 20 nm. They are monodispersed with no agglomeration due to the natural capping agents like phytochemicals present in the ZnO NP's. Therefore, no external capping agents were added to reduce the agglomeration; this reduced the use of toxic and expensive chemicals. Hence, this method is considered as one of the less expensive and environmentally friendly methods to prepare ZnO NP's.

The EDS image of ZnO NP's prepared by *Alchemilla vulgaris* (Lady's mantle) leaves is depicted in Fig. 4 (b). The qualitative and quantitative analysis of ZnO NP's were carried out using EDS. The atomic % of zinc and oxygen was found to be 50% each; which is very well matches with the theoretical values and they are stoichiometric to each other.

3.3. UV–visible spectroscopy

Fig. 5 shows the UV–visible spectrum of ZnO NP's prepared from *Alchemilla vulgaris* (Lady's mantle) leaves. It uses light in both near UV as well as in near-infrared ranges. Generally, the molecules undergo electronic transitions in the visible range and directly affect the perceived color of the chemicals involved (Shashanka and Ceylan, 2020). The green synthesized ZnO NP's were sonicated for 2 min in deionized water to get homogeneously dispersed ZnO nanoparticle solution. The sonicated ZnO solution depicts a sharp absorption peak at 362 nm as a result of surface plasmon absorption (SPA). The collective oscillation of the free conduction band electrons results in SPA when electromagnetic radiation colloid with them (Shashanka et al., 2019; Shashanka and Swamy, 2020). The result obtained from UV–Visible spectroscopy in this paper is comparable to the published reports of the authors elsewhere (Shashanka and Swamy, 2020; Shashanka et al., 2020).

The bandgap energy of the biosynthesized ZnO NP's were calculated using the following equation,

$$\mathrm{E} = \frac{\mathrm{h} \times \mathrm{C}}{\lambda} \tag{2}$$

where E = Bandgap energy
h = Planks constant
C = Speed of light
λ = Cut off wavelength

The intrinsic bandgap energy of 3.43 eV was obtained for cauliflower shaped ZnO NP's. The presently reported bandgap value of ZnO NP's is high compared to the published articles elsewhere (Angélica et al., 2016; Senthilkumar et al., 2017; Alamdari et al., 2020). This is due to the nanostructure of the biosynthesized ZnO and this resulted in the gradual decrease in the confined (Davis et al., 2019).

3.4. FTIR analysis

The spectrum depicts a strong broad peak at 3500 cm^{-1} which attributes the hydroxyl (O-H) group comprised of stretching and bending vibrations (Mishra et al., 2013). The IR peak at

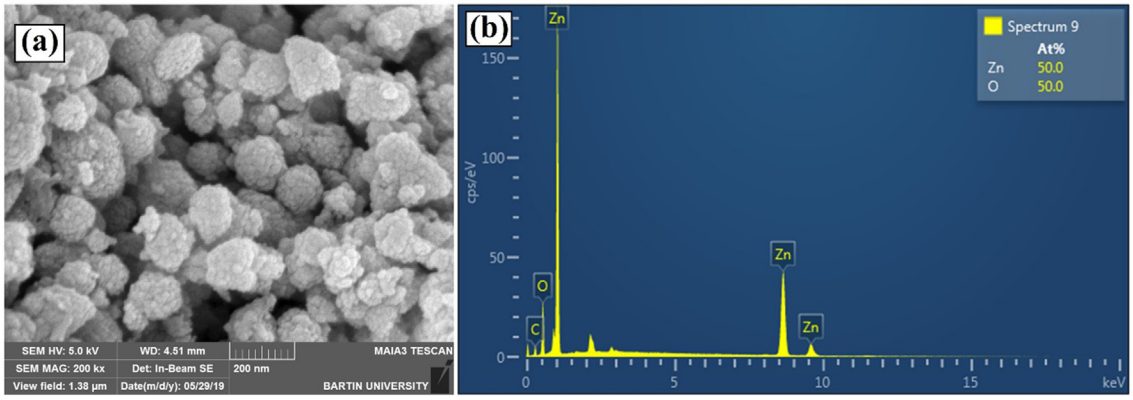

Fig. 4 **(a)** SEM image **(b)** Energy dispersed spectroscopy (EDS) image of cauliflower shaped ZnO NP's prepared by *Alchemilla vulgaris* (Lady's mantle) leaves.

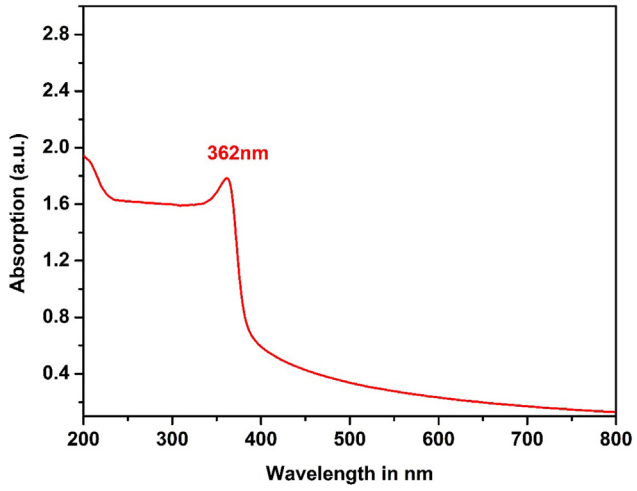

Fig. 5 UV–visible spectrum of ZnO NP's prepared from *Alchemilla vulgaris* (Lady's mantle) leaves.

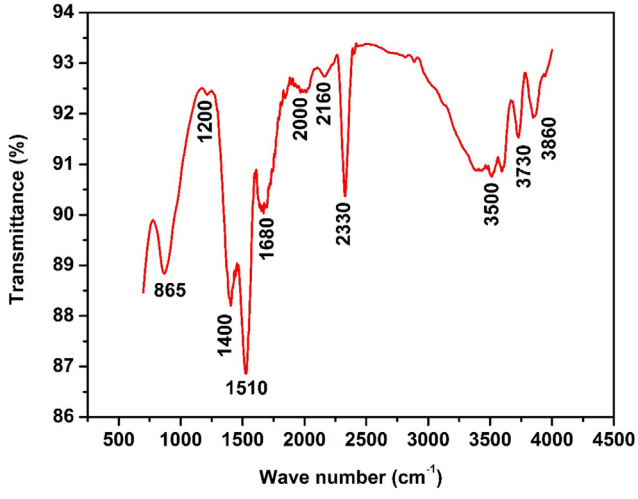

Fig. 6 The FTIR spectrum of biosynthesized ZnO NP's.

3730 cm^{-1} attributed by free hydroxyl group as shown in Fig. 6. The presence of stretching vibrations of polyphenols present in the extract substantiates the capping activity of surface of ZnO NP's. The presence of small sharp peaks between 2000 and 2200 cm^{-1} confirms the existence of amino acid (N–H) stretching (Venkateasan et al., 2017). The sharp and intense peaks at 1510 and 1400 cm^{-1} corresponds to the C = C group and are likely aroused due to the aromatic conjugates of the biomolecules present in the plant extract. IR bands at 1200 cm^{-1} and 865 cm^{-1} attributed to the C-O stretching vibration and the tetrahedral coordination of Zn respectively (Jayarambabu et al., 2015).

3.5. Investigation of particle size

The cumulative particle size distribution of ZnO NP's was successfully studied using particle size analyzer. Added the ZnO NP's to a pure solvent (water) and sonicated the same for 1 min to get the homogeneous dispersion of nanoparticles and later measured the particle size distribution. Fig. 7 shows the particle size distribution curve of biosynthesized ZnO

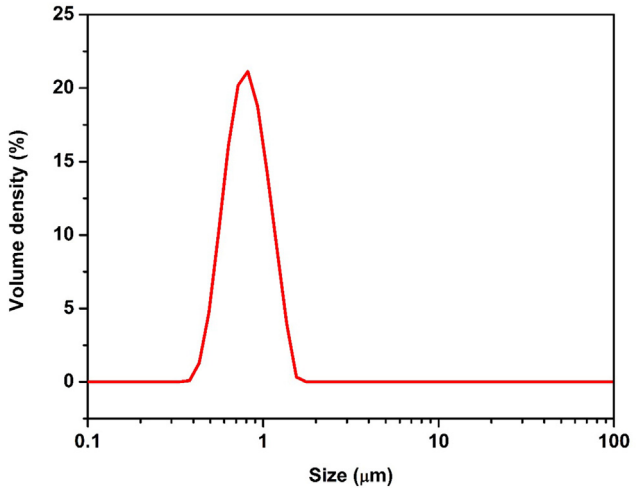

Fig. 7 The particle size distribution curve of green synthesized cauliflower shaped ZnO NP's.

NP's. The curve is slightly broad and confirming the different sized ZnO particles ranging from 250 nm to 1 μm. The particle size of maximum number of green synthesized ZnO NP's were around 550 nm as shown in the graph.

3.6. Thermal analysis

Thermal properties of biosynthesized ZnO NP's were investigated by TG and DTA at 6, 8, and 10℃/min heating rates between 30 and 1000℃ temperature as shown in Fig. 8 (a), 8 (b) and 8 (c) respectively. The prepared nanoparticles are thermally unstable over a temperature of 30–1000℃ and variation in heating rates. But, showed less weight loss after above 434℃ temperature at all the heating rates; in other words, the prepared ZnO NP's exhibited a great level of stability at higher temperature (after 434℃) (Arora et al., 2014). At 6℃/min, each 0.6% weight loss was observed at 111.5 and 252.1℃ respectively. The resultant weight loss is due to evaporation of water, decomposition of organic, and carbonaceous materials (Shashanka et al., 2020). This resulted in a total weight loss of 2.4% during 6℃/min heating rate. Similarly, during 8℃/min heating rate 7.1 and 2.5% of weight loss was observed at 338.1 and 707.7℃ respectively and a total of 10.1% weight loss was observed. At 10℃/min heating rate, a total of 3.5% weight loss was observed in which 1.7% weight loss at 302.4℃ and 0.9% weight loss at 769.5℃ was recorded respectively. These results confirmed that variation in the heating rate affects the amount of weight loss abruptly over a temperature of 30–1000℃ as shown in the figure. It is also confirmed that 6℃/min heating rate results in the lesser weight loss and therefore, the biosynthesized ZnO NP's show greater thermal stability at lower heating rates.

We studied the activation energy of ZnO NP's prepared from *Alchemilla vulgaris* (Lady's mantle) leaves using DTA as shown in Fig. 8 (a), 8 (b), and 8 (c) respectively. The green synthesized nanoparticles exhibit exothermic peaks at 666.4, 671.4 and 675.6℃ respectively at 6, 8, and 10℃/min heating rates. The ZnO nanophase is more stable at high temperatures due to the oxidative decomposition at higher temperatures which resulted in exothermic peaks. These decomposition peaks shift towards higher temperatures with an increase in heating rate as shown in the figure.

The activation energy of the biosynthesized ZnO NP's were calculated using Kissinger method (Kissinger, 1956). For more detail of method and calculation authors strongly recommend to refer their previous publications (Shashanka and Ceylan, 2020; Shashanka et al., 2020). The Kissinger equation is as follows;

$$ln\frac{\alpha}{T_P^2} = \frac{-E_c}{RT_P} + Constant \quad (4)$$

Where

T_P = Decomposition peak temperature,

α = Heating rate

R = Gas constant

Fig. 9 shows activation energy of the green synthesized ZnO NP's calculated from Kissinger equation and it was found to

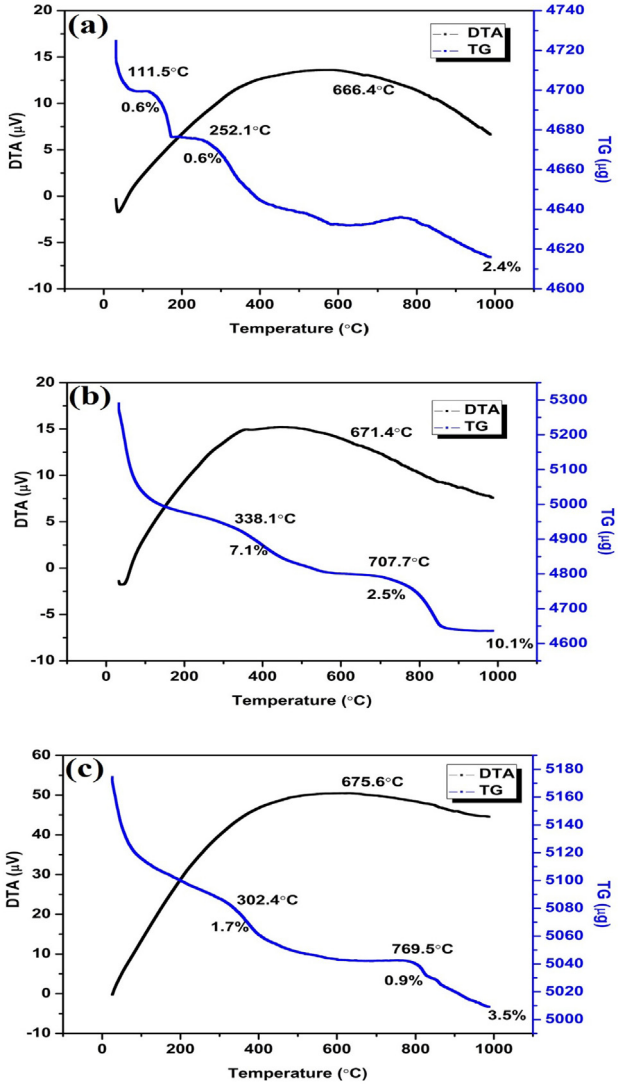

Fig. 8 The thermogravimetric analysis (TG) and differential thermal analysis (DTA) curve of biosynthesized nanoparticles at **(a)** 6 **(b)** 8, and **(c)** 10℃/min heating rates over a temperature range of 30–1000℃ respectively.

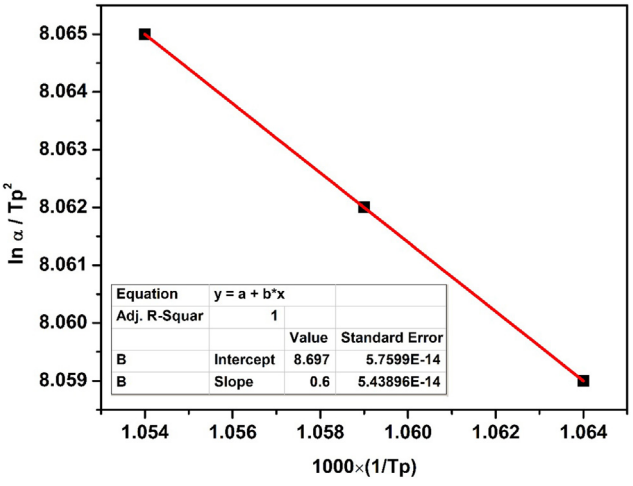

Fig. 9 The Kissinger plot of green synthesized ZnO NP's used to calculate the activation energy.

Table 2 The calculated values of activation energy of ZnO nanoparticles using Kissinger method.

Type of nanomaterial	Heating rate α (K/min)	Peak temperature T_P (K)	$\frac{\alpha}{T_P^2}$(X 10^{-4})	$\ln\frac{\alpha}{T_P^2}$	1000X$\frac{1}{T_P}$	Activation energy E_a (KJ/mol)
CuO nanoparticles	279	939.4	3.16	−8.059	1.064	12.92
	281	944.4	3.15	−8.062	1.059	
	283	948.6	3.14	−8.065	1.054	

be 12.92 kJ/moles. Table 2 represents the calculation of activation energy of ZnO NP's.

3.7. Inhibition of metabolic enzymes

AChE and BChE inhibition have been reported for the effective management of AD and the drugs act as cholinesterase inhibitors have recorded various benefits (Zengin et al., 2018). ZnO nanoparticle was very active in inhibiting AChE. The K_i value for AChE was determined to be 5.10 ± 0.47 μM (Table 3). The K_i value for Tacrine (TAC) molecule inhibitting AChE enzyme was determined to be 7.98 ± 1.76 μM. ZnO nanoparticle and TAC values IC_{50} were: ZnO nanoparticle (6.81 μM, r^2: 0.9067) < TAC (10.51 μM, r^2: 0.9983) for AChE. Similarly, the K_i values for BChE and the inhibiting property of TAC molecule was found to be 0.28 ± 0.03 and 0.80 ± 0.12 μM respectively (Table 3).

On the other hand, ZnO nanoparticle shown as IC_{50} and K_i values are 65.88 μM, r^2:0.9460, and 70.30 ± 7.92 (Table 3). The α-glycosidase assay exhibited that ZnO nanoparticle has shown an effective α-glycosidase inhibition than acarbose (IC_{50}: 71.11 μM, K_i: 85.88 ± 9.37). Consequently this has prompted the diabetes researchers to look for other potential therapies including α-glycosidase inhibitors (AGIs) to treat T1DM. Recently few reports indeed indicated that AGIs can also treat insulin deficiency caused by T1DM (Taslimi et al., 2017a, 2017b; Gülçin et al., 2019).

3.8. Optical properties and photocatalytic performance

Fig. 10 represents the optical properties and photo-catalytic testing results of as-synthesized ZnO NPs. In the graphs given in Fig. 10 (a) and 10 (b), the optical behavior of synthesized ZnO NPs, which has critical importance in photocatalytic reactions, has been examined. The wavelength versus absorption spectrum curve given in Fig. 10 (a) is obtained from converting the diffused reflectance (given inset of the graph) data of solid ZnO particles via the Kubelka-Munk (K-M) Reflectance Theory (Kubelka, 1931, 1948). The optical band gap value for as-synthesized ZnO NPs was estimated by using the Tauc method, given by the following equation (Tauc et al., 1966; Tauc, 1974):

$$\alpha h\nu = A(h\nu - E_g)^n \tag{5}$$

In the equation above, α, h, ν, A and E_g are extinction coefficient, which is proportional to F(R), Planck constant (J.s), light frequency (s^{-1}), proportionality constant and optical band gap of the material (eV), respectively. The value of the exponent n defines the nature of the electronic transition between the valence band and conduction band for semiconductor. It is well known in the literature that the band type of ZnO is an allowed direct transition (Özgür et al., 2015). Therefore, the estimated optical band gap value for as-synthesized ZnO nanoparticles was found to be 3.27 eV, as represented in Fig. 10 (b), by extrapolating the straight portion to the energy axis at α = 0.

The photocatalytic activities of ZnO NPs were investigated by monitoring the degradation rate of RhB in the presence of ZnO Photo-catalysts under an AM1.5 filtered light solar simulator. The absorption changes of organic dye molecules in an aqueous solution throughout the photo-catalytic test have been demonstrated in Fig. 11 (a) at indicated interval times. As per Beer-Lambert Law, the maximum absorbance value of obtained peaks should gradually decrease depending on the remaining organic molecule concentration in the solution with taking place the photodegradation reactions in the presence of Photo-catalyst under solar irradiation. Therefore, determining the degradation rate of degraded RhB in the photo-catalytic process was calculated using Beer-Lambert equation (Swinehart, 1962):

Table 3 The enzyme inhibition results of ZnO nanoparticle against butyrylcholinesterase (BChE), achethylcholinesterase (AChE) and α-glycosidase (α-Gly) enzymes.

Compounds	IC_{50} (μM) K_i (μM)								
	BChE	r^2	AChE	r^2	α-Gly	r^2	BChE	AChE	α-Gly
Zn nanoparticle	0.34	0.9348	6.81	0.9067	65.88	0.9460	0.28 ± 0.03	5.10 ± 0.47	70.30 ± 7.92
TAC**	0.88	0.9295	10.51	0.9983	–	–	0.80 ± 0.12	7.98 ± 1.76	–
ACR***	–	–	–	–	71.11	0.9406	–	–	85.88 ± 9.37

**Tacrine (TAC) was used as a control for AChE and BChE enzymes.
***Acarbose (ACR) was used as a control for α-glycosidase enzyme.

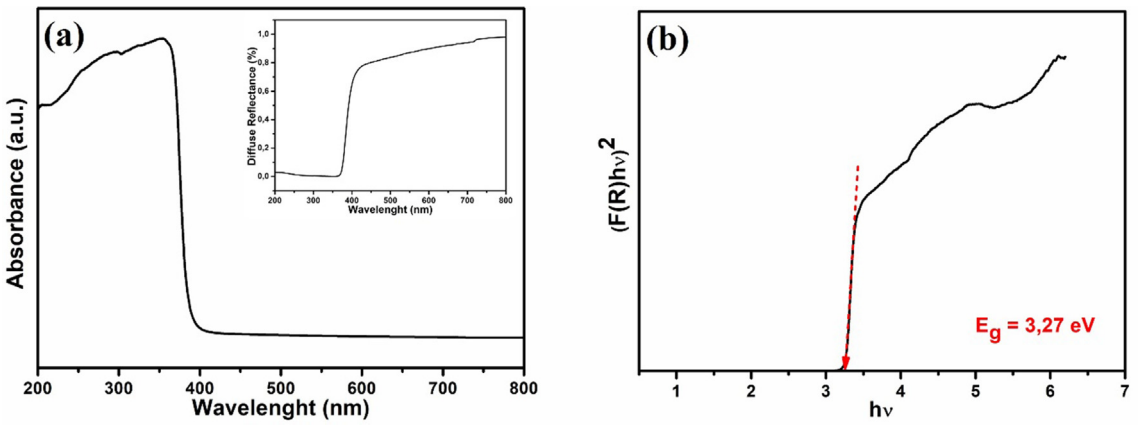

Fig. 10 **(a)** UV–Vis-NIR absorption spectrum of the as-synthesized ZnO derived from the diffused reflectance spectrum (given at inner graphic) **(b)** the determination of optical band gap value for the as-synthesized ZnO by using Tauc approximation. (E_g, defines an optical band gap of ZnO particles).

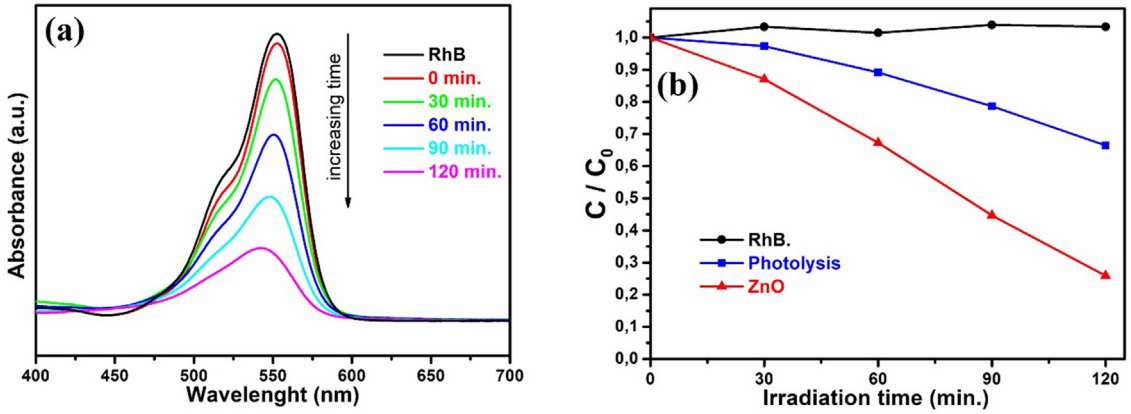

Fig. 11 **(a)** UV–vis absorption spectra of photodegraded RhB solutions during photo-catalytic experiment at given time intervals **(b)** Photodegradation ratio vs irradiation times for as-synthesized ZnO along with the photolysis of RhB, which is calculated by using Beer-Lambert Law at indicated time intervals (30 min.) (C_0 indicates the initial concentration of RhB and C_t indicates concentration of RhB at indicated irradiation time intervals).

$$A = \varepsilon l c \tag{6}$$

where A is absorbance, ε is absorption coefficient, l is the length of the beam in the medium and c is the concentration of the absorbing species in the medium.

By utilizing Beer-Lambert Law, the real-time degradation curves of RhB as a function of irradiation time have been given in Fig. 11 (b) via converting absorption values at the indicated time to concentration. For good surveillance of the performance of as-synthesized ZnO Photo-catalysts, photolysis of RhB under solar illumination (black curve), photolysis of RhB in the presence of H_2O_2 without any catalysts (blue curve), and photodegradation of RhB with synthesized ZnO Photo-catalysts are presented in Fig. 11 (b). Zero minutes in Fig. 11 indicate the starting point of solar irradiation time after establishing the adsorption/desorption equilibrium on the surface of the ZnO nanoparticles in the dark.

Since organic compounds can be decomposed by ultraviolet light, a reference test, shown as a black curve in Fig. 11 (b), was conducted in order to determine the decomposition of RhB for 2 h under solar irradiation and as a result, no degradation could be observed. The powerful oxidizing agent, such as hydroxyl radicals (•OH), are generated to treat contaminated waters in the method of an advanced oxidation processes (AOPs) (Glaze et al., 1987). In process of the photolysis of H_2O_2 (H_2O_2/UV), hydrogen peroxide can be photolyzed to lead producing a highly reactive and nonselective oxidizing agent, such as hydroxyl radicals, by radiation at wavelengths of about 250 nm (Guittonneau et al., 1990). The possible photocatalytic mechanism of ZnO powders against RhB dye is shown in Fig. 12. A decolorization of an organic compound by photolysis of H_2O_2, adding 0.5 mL H_2O_2 into 80 mL solution in this experiment, is demonstrated as a blue curve in Fig. 11 (b) under the illumination of an AM1.5 solar simulator and the degradation rate of RhB is observed to be about 34% for illumination of 2 h. In the heterogeneous photocatalytic process, upon illumination, electrons (e^-) in conduction (CB) and holes (h^+) in valence bands (VB) are generated on the solid surfaces of semiconductor Photo-catalysts. The called Reactive Oxygen Species (ROS), such as singlet oxygen ($^1O_2$), superoxide anion radical ($^{\bullet}O_2^-$), hydrogen peroxide

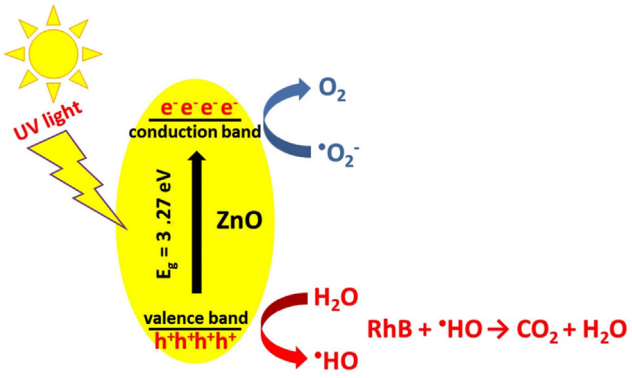

Fig. 12 The photocatalytic mechanism of ZnO powders against RhB dye.

(H_2O_2) and hydroxyl radical (•OH), are generated through the reactions with the photoinduced holes and electrons in the aquatic media naturally involving oxygen (Nosaka and Nosaka, 2017). The formation of ROS, resulting in taking place these reactions in aquatic media, plays a primary role in the organic degradation process in the heterogenous photocatalysis (Oturan and Aaron, 2014). Adsorption characteristic of as-synthesized ZnO nanoparticles, as seen in absorption vs wavelength graphic in Fig. 11 (a), is as low as about 3% of all RhB in aqueous solution. The degradation rate of RhB in presence of the as-synthesized ZnO Photo-catalysts particles is shown in a red curve [Fig. 11 (b)]. As demonstrated in figure, the degradation rate is seen to be about 75% of the RhB after illumination of 2 h, which is 2.2x more efficient than in the case of degradation by photolysis of H_2O_2. Table 4 depicts the photodegradation of various dyes using ZnO nanoparticles reported by various researchers in comparison with the present result.

4. Conclusion

Successfully synthesized cauliflower-shaped ZnO NPs by a simple, robust, and environmentally friendly one-pot biological method using *Alchemilla vulgaris* (Lady's mantle) leaves. The biosynthesized ZnO NPs exhibited broad XRD peaks even after calcination and this confirms its nano-crystallinity with an average size of 20 nm. SEM analysis confirmed the cauliflower shape of prepared ZnO NPs with an average size of 120 nm and each beads inside the cauliflower shape exhibit the average particle size of 20 nm. We have not used any capping or reducing agents externally. The IR band at 865 cm^{-1} attributed the tetrahedral coordination of Zn. The presence of stretching vibrations of polyphenols present in the extract substantiates the capping activity on the surface of ZnO NPs. The high percentage of prepared ZnO NPs exhibits a cumulative particle size of 550 nm. The TG analysis confirmed the abrupt variation in the total weight loss of 2.4%, 10.1% and 3.5% was observed at 6, 8, and 10℃/min heating rates respectively and this confirms that, the biosynthesized ZnO NPs shows greater thermal stability at lower heating rates. The green synthesized ZnO NPs show exothermic peaks at 666.4, 671.4 and 675.6℃ respectively at 6, 8, and 10℃/min heating rates. The decomposition peak of ZnO NPs shifts towards higher temperatures with an increase in heating rate where ZnO nanophase becomes more stable. The activation energy of the cauliflower-shaped ZnO NPs was calculated by Kissinger method and it was found to 12.92 kJ/moles. The biosynthesized ZnO NPs showed excellent inhibition effects on AChE, BChE, and α-glycosidase enzymes activities even at low micromolar concentrations. We believe that these results may be useful in the synthesis of new metabolic enzymes inhibitors and in the development of drugs for the treatment of some diseases. The bandgap value was calculated by two different methods and the values were found to be slightly differ-

Table 4 Photodegradation of various dyes using ZnO reported by various researchers.

Samples	Morphology	Energy band gap (eV)	Material used to photodegradation	Photodegradation efficiency (%)	References
PVA capped ZnO	Spherical	3.57	RR141 azo dye	42	(Kakarndee and Nanan 2018)
ZnO nanoparticles	Hexagonal	3.20	RR141 azo dye	95	(Chankhanittha and Nanan 2018)
SDS-capped ZnO	Hexagonal	3.20	RR141 azo dye	90	(Juabrum et al., 2019)
ZnO/Bi_2MoO_6	Flower	3.25	Rhodamine B (RhB)	92	(Chankhanittha and Nanan 2021)
ZnO/CdS nanocomposite	Spherical	3.24/2.41	RR141 azo dye	80	(Senasu et al., 2021)
ZnO/CdS nanocomposite	Spherical	3.24/2.41	ofloxacin (OFL) antibiotic,	73	(Senasu et al., 2021)
ZnO nanocatalyst	Mixed shape		Malachite green	96	(Maureen et al., 2019)
ZnO nanoparticles	Spherical	3.30	Methylene Blue and Rhodamine B		(Blažeka et al., 2020)
ZnO nanoparticles	Cauliflower	3.27	Rhodamine B (RhB)	75	(Present paper)

ent from each other, as determined 3.43 and 3.27 eV, respectively.. The cauliflower-shaped ZnO photocatalysts synthesized by *Alchemilla Vulgaris* leaves extract exhibited good photocatalytic activity in the degradation of organic molecules (RhB) in aqueous media under AM1.5 solar illumination.

Declaration of Competing Interest

The authors declare that they have no known competing financial interests or personal relationships that could have appeared to influence the work reported in this paper.

Acknowledgment

The authors gratefully acknowledge Bartin University Scientific Research Projects Unit, Turkey for providing financial support to conduct the research (Project number: 2019-FEN-A-006).

References

Ahmed, S.N., Haider, W., 2018. Heterogeneous photocatalysis and its potential applications in water and wastewater treatment: a review. Nanotechnology. 29, 342001.

Alamdari, S., Ghamsari, M.S., Lee, C., Han, W., Park, H.-H., Tafreshi, M.J., Afarideh, H., Ara, M.H.M., 2020. Preparation and Characterization of Zinc Oxide Nanoparticles Using Leaf Extract of *Sambucus ebulus*. Appl. Sci. 10, 3620.

Angélica, S.-T., Patricia, A.-M., Pedro, P.-R., Wilber, A.-F., Mario, M.-Y., 2016. Optical Band Gap Estimation of ZnO Nanorods. Mater. Res. 19, 33–38.

Arora, A.K., Devi, S., Jaswal, V.S., Singh, J., Kinger, M., Gupta, V. D., 2014. Synthesis and characterization of ZnO nanoparticles. Orient. J. Chem. 30, 1671–1679.

Bala, N., Saha, S., Chakraborty, M., Maiti, M., Das, S., Basu, R., Nandy, P., 2015. Green synthesis of zinc oxide nanoparticles using Hibiscus subdariffa leaf extract: effect of temperature on synthesis, anti-bacterial activity and anti-diabetic activity. RSC Adv. 5, 4993–5003.

Bhuyan, T., Mishra, K., Khanuja, M., Prasad, R., Varma, A., 2015. Biosynthesis of zinc oxide nanoparticles from *Azadirachta indica* for antibacterial and photocatalytic applications. Mater. Sci. Semicond. Process. 32, 55–61.

Biçer, A., Taslimi, P., Yakalı, G., Gülcin, I., Gültekin, M.S., Cin, G. T., 2019. Synthesis, Characterization, Crystal Structure of Novel Bis-Thiomethylcyclohexanone Derivatives and their Inhibitory Properties against Some Metabolic Enzymes. Bioorg. Chem. 82, 393–404.

Blažeka, D., Car, J., Klobucar, N., Jurov, A., Zavašnik, J., Jagodar, A., KovaceviC, E., Krstulovic, N., 2020. Photodegradation of Methylene Blue and Rhodamine B Using Laser-Synthesized ZnO Nanoparticles. Materials. 13, 4357.

Boroja, T., Mihailović, V., Katanić, J., Pan, S.-P., Nikles, S., Imbimbo, P., Monti, D.M., Stanković, N., Stanković, M.S., Bauer, R., 2018. The biological activities of roots and aerial parts of Alchemilla vulgaris L. S. Afr. J. Bot. 116, 175–184.

Chankhanittha, T., Nanan, S., 2018. Hydrothermal synthesis, characterization and enhanced photocatalytic performance of ZnO toward degradation of organic azo dye. Mater. Lett. 226, 79–82.

Chankhanittha, T., Watcharakitti, J., Nanan, S., 2019. PVP-assisted synthesis of rod-like ZnO photocatalyst for photodegradation of reactive red (RR141) and Congo red (CR) azo dyes. J. Mater. Sci.: Mater. Electron. 30, 17804–17819.

Chankhanittha, T., Nanan, S., 2021. Visible-light-driven photocatalytic degradation of ofloxacin (OFL) antibiotic and Rhodamine B (RhB) dye by solvothermally grown ZnO/Bi2MoO6 heterojunction. J. Colloid Interface Sci. 582, 412–427.

Chankhanittha, T., Somaudon, V., Photiwat, T., Youngme, S., Hemavibool, K., Nanan, S., 2021a. Enhanced photocatalytic performance of ZnO/Bi_2WO_6 heterojunctions toward photodegradation of fluoroquinolone-based antibiotics in wastewater. J. Phys. Chem. Solids 153, 109995–110015.

Chankhanittha, T., Yenjai, C., Nanan, S., 2021b. Utilization of formononetin and pinocembrin from stem extract of *Dalbergia parviflora* as capping agents for preparation of ZnO photocatalysts for degradation of RR141 azo dye and ofloxacin antibiotic. Catal. Today. https://doi.org/10.1016/j.cattod.2021.03.002.

Datta, A., Patra, C., Bharadwaj, H., Kaur, S., Dimri, N., Khajuria, R., 2017. Green Synthesis of Zinc Oxide Nanoparticles Using *Parthenium hysterophorus* Leaf Extract and Evaluation of their Antibacterial Properties. J Biotechnol Biomater. 7, 1000271.

Davis, K., Yarbrough, R., Froeschle, M., White, J., Rathnayake, H., 2019. Band gap engineered zinc oxide nanostructures via a sol–gel synthesis of solvent driven shape controlled crystal growth. RSC Adv. 9, 14638–14648.

Dogan, S.S., Kocabas, A., 2020. Green synthesis of ZnO nanoparticles with Veronica multifida and their antibiofilm activity. Hum. Exp. Toxicol. 39, 319–327.

Ellman, G., Courtney, K., Andres, V., Featherston, R., 1961. A new and rapid colorimetric determination of acetylcholinesterase activity. Biochem. Pharmacol. 7, 88–95.

Erdemir, F., Celepci, D.B., Aktaş, A., Gök, Y., Kaya, R., Taslimi, P., Demir, Y., Gülçin, I., 2019. Novel 2-aminopyridine liganded Pd(II) N-heterocyclic carbene complexes: synthesis, characterization, crystal structure and bioactivity properties. Bioorg. Chem. 91, 103134.

Ezealisiji, K.M., Noundou, X.S., Maduelosi, B., Nwachukwu, N., Krause, R.W.M., 2019. Green synthesis of zinc oxide nanoparticles using Solanum torvum (L) leaf extract and evaluation of the toxicological profle of the ZnO nanoparticles–hydrogel composite in Wistar albino rats. International Nano Letters. 9, 99–107.

Fu, L., Fu, Z., 2015. Plectranthus amboinicus leaf extract–assisted biosynthesis of ZnO nanoparticles and their photocatalytic activity. Ceram. Int. 41, 2492–2496.

Glaze, W.H., Kang, J.W., Chapin, D.H., 1987. The chemistry of water treatment processes involving ozone, hydrogen peroxide and ultraviolet radiation. Ozone Sci. Eng. 9, 335–352.

Guittonneau, S., De Laat, J., Duguet, J.P., Bonnel, C., Dore, M., 1990. Oxidation of parachloronitrobenzene in dilute aqueous solution by O_3 + UV and H_2O_2 + UV: a comparative study. Ozone: Science & Engineering: The Journal of the International Ozone Association. 12, 73–94.

Gulçin, I., Taslimi, P., Aygün, A., Sadeghian, N., Bastem, E., Kufrevioglu, O.I., Turkan, F., Şen, F., 2018. Antidiabetic and antiparasitic potentials: Inhibition effects of some natural antioxidant compounds on α-glycosidase, α-amylase and human glutathione S-transferase enzymes. Int. J. Biol. Macromol. 119, 741–746.

Gülçin, I., Tel, A.Z., Gören, A.C., Taslimi, P., Alwasel, S., 2019. Sage (Salvia pilifera): Determination its polyphenol contents, anticholinergic, antidiabetic and antioxidant activities. J. Food Meas. Charact. 13, 2062–2074.

Gültekin, D.D., Güngör, A.A., Önem, H., Babagil, A., Nadaroğlu, H., 2016. Synthesis of Copper Nanoparticles Using a Different Method: Determination of Its Antioxidant and Antimicrobial Activity. Journal of the Turkish Chemical Society Section A: Chemistry. 3, 623–636.

Gupta, S., Shashanka, R., Chaira, D., 2015. Synthesis of nanostructured duplex and ferritic stainless steel powders by planetary milling: an experimental and simulation study. IOP Conf. Ser. Mater. Sci. Eng. 75, 12033.

Hareesha, N., Manjunatha, J.G., Raril, C., Tigari, G., 2019. Sensitive and Selective Electrochemical Resolution of Tyrosine with Ascor-

bic Acid through the Development of Electropolymerized Alizarin Sodium Sulfonate Modified Carbon Nanotube Paste Electrodes. ChemistrySelect. 4, 4559–4567.
Huseynova, M., Medjidov, A., Taslimi, P., Aliyeva, M., 2019. Synthesis, Characterization, Crystal Structure of the Coordination Polymer Zn(II) with Thiosemicarbazone of Glyoxalic Acid and Their Inhibitory Properties Against Some Metabolic Enzymes. Bioorg. Chem. 83, 55–62.
Jayarambabu, N., Kumari, B.S., Rao, K.V., Prabhu, Y.T., 2015. Beneficial role of zinc oxide nanoparticles on green crop production. International Journal of Multidisciplinary Advanced Research Trends. 2, 273–282.
Jiang, J., Pi, J., Cai, J., 2018. The Advancing of Zinc Oxide Nanoparticles for Biomedical Applications. Bioinorg. Chem. Appl. 2018, 1062562.
Juabrum, S., Chankhanittha, T., Nanan, S., 2019. Hydrothermally grown SDS-capped ZnO photocatalyst for degradation of RR141 azo dye. Mater. Lett. 245, 1–5.
Kakarndee, S., Nanan, S., 2018. SDS capped and PVA capped ZnO nanostructures with high photocatalytic performance toward photodegradation of reactive red (RR141) azo dye. J. Environ. Chem. Eng. 6, 74–94.
Kissinger, H.E., 1956. Variation of Peak Temperature with Heating Rate in Differential Thermal Analysis. J Res Natl Bur Stand. 57, 217–221.
Knoll, B., Keilmann, F., 1999. Near-field probing of vibrational absorption for chemical microscopy. Nature 399, 134–137.
Kubelka, P., 1931. Ein Beitrag zur Optik der Farbanstriche (Contribution to the optic of paint). Z. Tech. Phys. 12, 593–601.
Kubelka, P., 1948. New contributions to the optics of intensely light-scattering materials. Part I, Josa. 38, 448–457.
Küçükoğlu, K., Gül, H.I., Taslimi, P., Gülçin, I., Supuran, C.T., 2019. Investigation of inhibitory properties of some hydrazone compounds on hCA I, hCA II and AChE enzymes. Bioorg. Chem. 86, 316–321.
Kuzu, B., Tan, M., Taslimi, P., Gülçin, I., Taspınar, M., Menges, N., 2019. Mono- or di-substituted imidazole derivatives for inhibiton of acetylcholine and butyrylcholine esterases. Bioorg. Chem. 86, 187–196.
Liz-Marzán, L.M., Giersig, M., Mulvaney, P., 1996. Synthesis of nanosized gold-silica coreshell particles. Langmuir 12, 4329–4335.
Mehar, S., Khoso, S., Qin, W., Anam, I., Iqbal, A., Iqbal, K., 2019. Green Synthesis of Zincoxide Nanoparticles from *Peganum harmala*, and its biological potential against bacteria. Front Nanosci Nanotech. 6, 1–5.
Mirzaeia, H., Darroudi, M., 2017. Zinc oxide nanoparticles: Biological synthesis and biomedical applications. Ceram. Int. 43, 907–914.
Mishra, M., Paliwal, J.S., Singh, S.K., Selvarajan, E., Subathradevi, C., Mohanasrinivasan, V., 2013. Studies on the Inhibitory Activity of Biologically Synthesized and Characterized Zinc Oxide Nanoparticles using Lactobacillus sporogens against Staphylococcus aureus. J Pure Appl Microbiol. 7, 1–6.
Maureen, C.-O.O., Nnaemeka, O.J., Basil, A.N., Emeka, O.E., 2019. Photocatalytic Degradation of a Basic Dye Using Zinc Oxide Nanocatalyst. International Letters of Chemistry, Physics and Astronomy. 81, 18–26.
Nayak, A.K., Shashanka, R., Chaira, D., 2016. Effect of nanosize yittria and tungsten addition to duplex stainless steel during high energy planetary milling. IOP Conf. Ser. Mater. Sci. Eng. 115, 12008.
Nosaka, Y., Nosaka, A.Y., 2017. Generation and detection of reactive oxygen species in photocatalysis. Chem. Rev. 117, 11302–11336.
Oturan, M.A., Aaron, J.J., 2014. Advanced oxidation processes in water/wastewater treatment: principles and applications. A review. Critical Reviews in Environmental Science and Technology. 44, 2577–2641.
Özgür, Ü., Alivov, Y.I., Liu, C., Teke, A., Reshchikov, M., Doğan, S., Avrutin, V.C.S.J., Cho, S.J., Morkoç, A.H., 2015. A comprehensive review of ZnO materials and devices. J. Appl. Phys. 98, 041301.
Rahaiee, S., Ranjbar, M., Azizi, H., Govahi, M., Zare, M., 2020. Green synthesis, characterization, and biological activities of saffron leaf extract-mediated zinc oxide nanoparticles: A sustainable approach to reuse an agricultural waste. Appl. Organomet. Chem. 34, e5705.
Rajendrachari, S., Swamy, B.E.K., Reddy, S., Chaira, D., 2013. Synthesis of Silver Nanoparticles and their Applications. Anal. Bioanal. Electrochem. 5, 455–466.
Reddy, S., Swamy, B.E.K., Aruna, S., Kumar, M., Shashanka, R., Jayadevappa, H., 2012. Preparation of NiO/ZnO hybrid nanoparticles for electrochemical sensing of dopamine and uric acid. Chemical Sensors. 2, 1–7.
Santhoshkumar, J., Kumar, S.V., Rajeshkumar, S., 2017. Synthesis of zinc oxide nanoparticles using plant leaf extract against urinary tract infection pathogen. Resour.-Effic. Technol. 3, 459–465.
Selim, Y.A., Azb, M.A., Ragab, I., Abd El-Azim, M.H.M., 2020. Green Synthesis of Zinc Oxide Nanoparticles Using Aqueous Extract of Deverra tortuosa and their Cytotoxic Activities. Sci. Rep. 10, 3445.
Senasu, T., Chankhanittha, T., Hemavibool, K., Nanan, S., 2021. Visible-light-responsive photocatalyst based on ZnO/CdS nanocomposite for photodegradation of reactive red azo dye and ofloxacin antibiotic. Mater. Sci. Semicond. Process. 123, 105558.
Senthilkumar, N., Nandhakumar, E., Priya, P., Soni, D., Vimalan, M., Potheher, I.V., 2017. Synthesis of ZnO nanoparticles using leaf extract of Tectona grandis (L.) and their anti-bacterial, anti-arthritic, anti-oxidant and in vitro cytotoxicity activities. New J. Chem. 41, 10347–10356.
Sharmila, G., Thirumarimurugan, M., Muthukumaran, C., 2019. Green synthesis of ZnO nanoparticles using *Tecoma castanifolia* leaf extract: Characterization and evaluation of its antioxidant, bactericidal and anticancer activities. Microchem. J. 145, 578–587.
Shashanka, R., Chaira, D., 2014. Phase transformation and microstructure study of nano-structured austenitic and ferritic stainless steel powders prepared by planetary milling. Powder Technol. 259, 125–136.
Shashanka, R., Chaira, D., Swamy, B.E.K., 2015a. Electrochemical investigation of duplex stainless steel at carbon paste electrode and its application to the detection of dopamine, ascorbic and uric acid. Int. J. Sci. Eng. Res. 6, 1863–1871.
Shashanka, R., Chaira, D., 2015a. Development of nano-structured duplex and ferritic stainless steel by pulverisette planetary milling followed by pressureless sintering. Mater. Char. 99, 220–229.
Shashanka, R., Chaira, D., 2015b. Optimization of milling parameters for the synthesis of nano-structured duplex and ferritic stainless steel powders by high energy planetary milling. Powder Technol. 278, 35–45.
Shashanka, R., Chaira, D., Swamy, B.E.K., 2015b. Electrocatalytic response of duplex and yittria dispersed duplex stainless steel modified carbon paste electrode in detecting folic acid using cyclic voltammetry. Int. J. Electrochem. Sci. 10, 5586–5598.
Shashanka, R., Chaira, D., Swamy, B.E.K., 2016. Fabrication of yttria dispersed duplex stainless steel electrode to determine dopamine, ascorbic and uric acid electrochemically by using cyclic voltammetry. Int. J. Sci. Eng. Res. 7, 1275–1285.
Shashanka, R., 2017. Synthesis of nano-structured stainless steel powder by mechanical alloying-an overview. Int. J. Sci. Eng. Res. 8, 588–594.
Shashanka, R., 2019. Non-lubricated dry sliding wear behavior of spark plasma sintered nano-structured stainless steel. J. Mater. Environ. Sci. 10, 767–777.
Shashanka, R., Kamacı, Y., Tas¸ R., Ceylan, Y., Bülbül, A.S., Uzun, O., Karaoglanli, A.C., 2019. Antimicrobial investigation of CuO and ZnO nanoparticles prepared by a rapid combustion method. Phy. Chem. Res. 7, 799-812.
Shashanka, R., Ceylan, K.B., 2020. The activation energy and antibacterial investigation of spherical Fe_3O_4 nanoparticles prepared by *Crocus sativus* (Saffron) flowers. Biointerface Research in Applied Chemistry. 10, 5951–5959.

Shashanka, R., Swamy, B.E.K., 2020. Biosynthesis of silver nanoparticles using leaves of Acacia melanoxylon and its application as dopamine and hydrogen peroxide sensors. Phy. Chem. Res. 8, 1–18.

Shashanka, R., Yilmaz, V.M., Karaoglanli, A.C., Uzun, O., 2020a. Investigation of activation energy and antibacterial activity of CuO nano-rods prepared by Tilia Tomentosa (Ihlamur) leaves. Moroccan Journal of Chemistry. 8, 497–509.

Shashanka, R., 2020. Investigation of optical and thermal properties of CuO and ZnO nanoparticles prepared by Crocus Sativus (Saffron) flower extract. J. Iran. Chem. Soc. https://doi.org/10.1007/s13738-020-02037-3.

Shashanka, R., Esgin, H., Yilmaz, V.M., Caglar, Y., 2020b. Fabrication and characterization of green synthesized ZnO nanoparticle based dye-sensitized solar cells. J. Sci.: Adv. Mater. Devices 5, 185–191.

Swinehart, D.F., 1962. The beer-lambert Law. J. Chem. Educ. 39, 333.

Tao, Y., Zhang, Y., Cheng, Y., Wang, Y., 2013. Rapid screening and identification of α-glucosidase inhibitors from mulberry leaves using enzyme-immobilized magnetic beads coupled with HPLC/MS and NMR. Biomed. Chromatogr. 27, 148–155.

Taslimi, P., Caglayan, C., Gulçin, I., 2017a. The impact of some natural phenolic compounds on carbonic anhydrase, acetylcholinesterase, butyrylcholinesterase, and α-glycosidase enzymes: an antidiabetic, anticholinergic, and antiepileptic study. J. Biochem. Mol. Toxicol. 31, e21995.

Taslimi, P., Akıncıoğlu, H., Gulçin, I., 2017b. Synephrine and phenylephrine act as α-amylase, α-glycosidase, acetylcholinesterase, butyrylcholinesterase and carbonic anhydrase enzymes inhibitors. J. Biochem. Mol. Toxicol. 31, e21973.

Taslimi, P., Gulçin, I., 2018. Antioxidant and anticholinergic properties of olivetol. J. Food Biochem. 42, e12516.

Taslimi, P., Aslan, H.E., Demir, Y., Oztaskin, N., Maraş, A., Gulçin, I., Beydemir, S., Goksu, S., 2018. Diarilmethanon, bromophenols and diarilmetan compounds: Discovery of potent aldose reductase, α-amylase and α-glycosidase inhibitors as new therapeutic approach in diabetes and functional hyperglycemia. Int. J. Biol. Macromol. 119, 857–863.

Tauc, J., 1974. Optical properties of amorphous semiconductors. Amorphous and Liquid Semiconductors. Springer, Boston, MA, pp. 159–220.

Tauc, J., Grigorovici, R., Vancu, A., 1966. Optical properties and electronic structure of amorphous germanium. Phys. Status Solidi. 15, 627–637.

Tobyn, G., Denham, A., Whitelegg, M., 2011. Alchemilla vulgaris, lady's mantle. Med Herbs. Elsevier.

Vahidi, A., Vaghari, H., Najian, Y., Najian, M.J., Hoda, J.-M., 2019. Evaluation of three different green fabrication methods for the synthesis of crystalline ZnO nanoparticles using *Pelargonium zonale* leaf extract. Green Process. Synth, 8, 302–308.

Venkateasan, A., Prabakaran, R., Sujatha, V., 2017. Phytoextract-mediated synthesis of zinc oxide nanoparticles using aqueous leaves extract of Ipomoea pes-caprae (L).R.br revealing its biological properties and photocatalytic activity. Nanotechnol Environ. Eng. 8, 1–15.

Zengin, M., Genc, H., Taslimi, P., Kestane, A., Guclu, E., Ogutlu, A., Karabay, O., Gulçin, I., 2018. Novel Thymol Bearing Oxypropanolamine Derivatives as Potent Some Metabolic Enzyme Inhibitors-Their Antidiabetic. Anticholinergic and Antibacterial Potentials. Bioorganic Chemistry. 81, 119–126.